Electron Spin−Echo Envelope Modulation Spectrum of Azurin at X-Band

M. van Gastel,[†] J. W. A. Coremans,[†] L. J. C. Jeuken,[‡] G. W. Canters,[‡] and E. J. J. Groenen*[,†]

Centre for the Study of Excited States of Molecules, Huygens Laboratory, Leiden University, P.O. Box 9504, 2300 RA Leiden, The Netherlands, and Gorlaeus Laboratories, Leiden Institute of Chemistry, P.O. Box 9502, 2300 RA Leiden, The Netherlands

Received: December 19, 1997; In Final Form: March 17, 1998

Frozen solutions of azurin and of its mutant His117Gly in the presence of [^{15}N]imidazole have been investigated by 9 GHz three-pulse electron spin−echo envelope modulation (ESEEM) and two-dimensional ESEEM spectroscopy. It is found that the interaction of the unpaired electron with a backbone nitrogen leads to a sizable contribution to the ESEEM spectrum. This observation provides the clue to the interpretation of the ESEEM spectrum of the prototypical blue-copper site of azurin. The modulations stem largely from the interaction of the electron spin with three nitrogen nuclei. The quadrupole bands of the remote nitrogen of histidine-117 dominate the spectrum. Smaller but significant contributions result from the backbone nitrogen and the remote nitrogen of histidine-46. Simulations of the ESEEM spectra of azurin confirm this interpretation and yield complete hyperfine and quadrupole tensors for all three nitrogens. The significant contribution of the backbone nitrogen to the ESEEM spectra of azurin nicely brings out the delocalized character of the unpaired-electron wave function of the oxidized copper center.

I. Introduction

Electron paramagnetic resonance (EPR) spectroscopy has become a standard tool in the study of copper proteins. In the paramagnetic state every type of copper site in a protein has its characteristic EPR spectrum.[1] For blue-copper proteins the spectrum is almost axial, and at the usual X-band microwave frequency the copper hyperfine splitting is resolved in the $g_{\|}$ region. However, the interaction of the unpaired electron with other nuclei in the copper site often remains hidden under the EPR line. With related techniques such as electron nuclear double resonance (ENDOR) and electron spin−echo envelope modulation (ESEEM) it is possible to resolve such hyperfine interactions. The ESEEM technique was pioneered in the copper−protein field by Mims and Peisach.[2] From that time onward, this method has been extensively used in the study of copper proteins and copper histidine/imidazole complexes.[3−10] Almost without exception these studies were performed at X-band microwave frequencies and consequently dealt with the interaction of the unpaired electron spin with the nuclear spins of the so-called remote nitrogens of the copper ligating histidines or imidazoles, i.e., those imidazole nitrogens that are not coordinated to copper. For these remote nitrogens the hyperfine interaction is approximately 1−2 MHz,[11] a value that at X-band frequency almost fulfils the "exact-cancellation" condition.[12] For cancellation, when in one of the electron spin manifolds, the splitting of the nuclear-spin levels owing to the nuclear Zeeman interaction is nullified by that of the hyperfine interaction, modulations become deep, and the analysis of the ESEEM spectra of frozen solutions may simplify considerably. The ESEEM frequencies of the canceled manifold are mainly determined by the quadrupole interaction. Consequently, the ESEEM spectrum is commonly characterized by narrow, intense bands typically below 2 MHz. Of the other electron-spin manifold only one relatively shallow and broad feature is resolved in the ESEEM spectrum. This corresponds to the so-called $\Delta M_I = 2$ transition with a typical frequency of about 4 MHz. When the unpaired electron is coupled to more than one remote nitrogen, combination bands may show up. Such combination bands have been recognized in the frequency region between the quadrupole frequencies and the $\Delta M_I = 2$ frequency and, through spectral simulation, used to estimate the number of coordinated histidines.[13] Spectral simulations also yield quantitative information on the hyperfine and quadrupole interaction of the remote nitrogens.

In the blue-copper protein azurin the copper ion is coordinated by five ligands. Three ligands, the Nδ atoms of histidines-46 and -117 and the Sγ atom of cysteine-112, are strongly bound to the copper which almost resides in the plane formed by these ligands.[14,15] The ESEEM spectrum of azurin has been reported already in 1984.[16] At first sight the spectrum, shown in Figure 1a, conforms to the qualitative picture sketched above: intense bands below 2 MHz and broad bands around 4 MHz are visible. Consequently, as a first guess one would expect that only the two remote nitrogens of the ligating histidines contribute to the ESEEM spectrum of azurin. Nevertheless, to the best of our knowledge the azurin ESEEM spectrum has resisted interpretation as yet. Only for the blue-copper protein stellacyanin have the results of simulations been indicated,[17] and for the blue-copper sites in laccase and ascorbate oxidase simulations of the ESEEM spectra have been reported.[8]

As shown in Figure 1, and reported previously,[18] the ESEEM spectra of frozen solutions of azurin and of the mutant H117G after external addition of imidazole are largely similar. In the mutant one of the copper ligands, histidine-117, is replaced by glycine which leaves an aperture at the copper site.[19,20] This aperture is filled upon addition of potential metal ligands to the protein solution. The UV/vis and EPR spectra reveal that the blue-copper site is restored[20] when imidazole is added, and this restoration is apparently complete to the extent that also

* To whom correspodence should be adressed.
[†] Leiden University.
[‡] Leiden Institute of Chemistry.

S1089-5639(98)00584-2 CCC: $15.00
Published on Web 05/20/1998

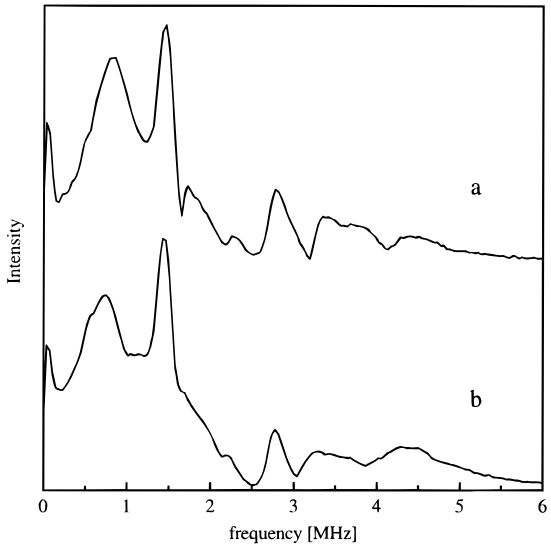

Figure 1. ESEEM spectra of frozen solutions of (a) azurin wild type and of (b) H117G ([^{14}N]imidazole). The spectra were measured at the high-field side of the ESE detected EPR spectra.

the ESEEM spectra of azurin and H117G(imidazole) are alike. This observation makes it possible to disentangle the difficult ESEEM spectrum of azurin through the use of the H117G mutant with [^{15}N]imidazole instead of [^{14}N]imidazole.

Here we report one- and two-dimensional ESEEM spectra of azurin and H117G([^{15}N]imidazole). A detailed interpretation of the ESEEM spectra is presented on the basis of spectral simulations. It is found that the contributions of the remote nitrogen of histidine-117 dominate the ESEEM spectra of azurin. The remote nitrogen of histidine-46, the other copper ligating histidine, makes a small contribution to the azurin ESEEM spectra as its hyperfine interaction is further from cancellation than that of the remote nitrogen of histidine-117. With the aid of the ESEEM spectra of H117G([^{15}N]imidazole) and the 2D-ESEEM spectra a quadrupole band of a backbone nitrogen in the ESEEM spectra of azurin is recognized and distinguished from combination bands. The presence of ESEEM bands of this backbone nitrogen, most probably that of cysteine-112, in the spectra of azurin brings out the delocalized character of the wave function of the unpaired electron and shows that in the analysis of the ESEEM spectra of blue-copper proteins not only contributions of remote nitrogens of coordinating histidines should be considered.

II. Materials and Methods

The purification of azurin from *Pseudomonas aeruginosa* and the preparation of the mutant H117G were reported previously.[19,21] Solutions of H117G([^{15}N]imidazole) were prepared by adding excess [^{15}N]imidazole (A. R. C. Labs, Amsterdam) to H117G solutions. The solutions of H117G([^{15}N]imidazole) and azurin wild type were buffered to pH 8 and 6.2, respectively, and the concentration of protein in the solution was typically 3 mM. The experiments on azurin were performed on solutions containing 40 vol % glycerol.

Three-pulse ESEEM and two-dimensional ESEEM experiments were performed at 6 K on a Bruker ESP380E X-band spectrometer. The time τ between the first two pulses was typically 144 ns, while a few experiments were performed at higher values. The starting value of the time T between the second and third pulse was 56 ns. The time increment between two consecutive T values was 8 ns, and in total 2048 data points were acquired. For 2D ESEEM, 128 × 1024 data points were acquired in the τ and T directions, respectively. The starting values of τ and T were 120 ns and 56 ns. A four-step phase cycling routine was used.[22] The microwave frequency was 9.748 GHz for azurin and 9.670 GHz for H117G([^{15}N]-imidazole). The three $\pi/2$ pulses had a width of 16 ns. Both the in-phase and the out-of-phase components of the stimulated echo were recorded, as well as the zero level of the echo. No dead-time reconstruction was performed with the Hankel singular value decomposition (HSVD) method. De Beer and van Ormondt showed that for single crystals with a discrete distribution of frequencies in the ESEEM spectra the modulation pattern is made up of a finite number of damped sinusoids.[23] Furthermore, they indicated that for frozen solutions the modulations may be described by damped sinusoids but the amplitudes, phases, and frequencies of the sinusoids lose their physical significance which removes the basis for the dead-time reconstruction. The modulation depth of all ESEEM spectra was normalized. To do so, the modulation pattern was corrected for the zero level of the echo and the decay was approximated by a Gaussian. The Gaussian was extrapolated to $T = 0$ and the modulation pattern rescaled in such a way that the amplitude of the Gaussian at $T = 0$ was equal to 100. Before the modulation pattern was transformed to the frequency domain, the background was removed by subtracting the Gaussian. No window function was used to avoid deformation of the spectrum. All ESEEM spectra shown are magnitude spectra.

III. Simulation Procedure

The ESEEM spectra of azurin arise from the coupling of more than one nitrogen nucleus (^{14}N, $I = 1$) to the unpaired electron spin ($S = {}^1/_2$). For frozen solutions all possible orientations of the external magnetic field, $\vec{B}_0$, with respect to a molecule are present. The ESEEM experiment is performed at a fixed magnetic field (B_{exp}), and only part of the orientations of $\vec{B}_0$ contribute to the modulation pattern. The first step in the simulations is to select those orientations of $\vec{B}_0$. To do so, the orientation of $\vec{B}_0$ is systematically varied with respect to a reference frame formed by the three principal axes of the **g**-tensor (xyz). Typically 3100 orientations of $\vec{B}_0$ are considered for each simulation. For each orientation of $\vec{B}_0$ and for each M_I state of copper the magnetic field of resonance (B_{res}) is calculated through diagonalization of the electron spin Hamiltonian. This Hamiltonian includes the electron Zeeman interaction and the copper hyperfine interaction (Cu, $I = {}^3/_2$):

$$H_e = \mu_\beta \vec{B}_0 \cdot \vec{\vec{g}} \cdot \vec{S} + S_z A_{zz}^{Cu} I_z^{Cu} \qquad (1)$$

where μ_β is the Bohr magneton and $\vec{\vec{g}}$ the **g**-tensor. Because the copper hyperfine interaction for $\vec{B}_0$ parallel to the z axis is resolved in the X-band EPR spectrum of azurin, this hyperfine interaction is included in the Hamiltonian (A_{zz}^{Cu}= 175 MHz). Only orientations of $\vec{B}_0$ for which B_{res} is calculated within an interval of 0.3 mT centered at B_{exp}, i.e., the magnetic field range spanned by the bandwidth of the microwave pulses, contribute to the modulation pattern. For a selected orientation, the eigenfunctions and eigenvalues of the nuclear-spin sublevels in both electron-spin manifolds (α, β) are calculated to obtain the ESEEM frequencies and amplitudes. The nuclear-spin Hamiltonian consists of the nuclear Zeeman interaction, the hyperfine interaction and, for the ^{14}N nuclei, the quadrupole interaction.

$$H_n = -g_N \beta_n \vec{I} \cdot \vec{B}_0 + \langle \vec{S} \rangle_{\alpha,\beta} \cdot \vec{\vec{A}} \cdot \vec{I} + \vec{I} \cdot \vec{\vec{Q}} \cdot \vec{I} \qquad (2)$$

where g_N is the nitrogen nuclear g-factor, β_n the nuclear Bohr magneton, $\langle\vec{S}\rangle_{\alpha,\beta}$ the expectation value of the electron-spin angular momentum operator in the α and β electron-spin manifold, respectively, $\vec{\vec{A}}$, the hyperfine, and $\vec{\vec{Q}}$ the quadrupole tensor. As first derived by Mims,[24,25] the contribution of a single nucleus to the three-pulse modulation function is given by:

$$Re\{V^{\alpha}(\tau, T) + V^{\beta}(\tau, T)\} = Re\{\sum_{ij,kl} M^{\dagger}_{ki} M_{il} M^{\dagger}_{lj} M_{jk}\, e^{-i(\omega^{\alpha}_{ij}+\omega^{\beta}_{kl})\tau}(e^{-i\omega^{\alpha}_{ij}T} + e^{-i\omega^{\beta}_{kl}T})\} \quad (3)$$

where M_{il} represents the transition probability between nuclear spin functions $|i_\alpha\rangle$ and $|l_\beta\rangle$ and ω^{α}_{ij} the frequency corresponding to the energy difference between $|i_\alpha\rangle$ and $|l_\beta\rangle$. The indices i, j and k, l run over the nuclear sublevels of the α and β electron-spin manifold, respectively. The modulation function of the α electron-spin manifold, $V^{\alpha}(\tau, T)$, contains all terms with $\omega^{\alpha}_{ij}T$ and that of the β electron-spin manifold, $V^{\beta}(\tau, T)$, all terms with $\omega^{\beta}_{ij}T$. When more than one nuclear spin interacts with the electron spin, the nuclear-spin Hamiltonian is diagonalized for each nucleus separately and the modulation function is obtained from the product rule. For a three-pulse experiment this becomes

$$V(\tau, T) = Re\{\prod_{i=1}^{N} V^{\alpha}_i(\tau, T) + \prod_{i=1}^{N} V^{\beta}_i(\tau, T)\} \quad (4)$$

where the product runs over the nuclei in interaction with the electron spin. The real part of the modulation function considered here corresponds to the in-phase component of the magnetization, while the imaginary part corresponds to the out-of-phase component. In the simulation program the complex amplitudes of the modulation function at the ESEEM frequencies are stored in a histogram. This allows, in principle, a direct comparison of simulated and experimental spectra. However, the intensities and line widths of the ESEEM bands in the experimental spectra are influenced by the following: (1) the decay of the echo, (2) the decay of the modulations, and (3) the experimental dead time. To account for these influences, the simulated frequency histogram is first transformed to the time domain; the real part of the time-domain data is taken and treated in the following way: (1) the zero-frequency component is multiplied by e^{-T/t_1} ($t_1 = 400$ μs), (2) the other frequencies are multiplied by e^{-T/t_2} ($t_2 = 4$ μs), and (3) the first points of the time-domain data up to 298 ns are removed from the data set. The values of t_1 and t_2 were chosen such that the decay of the modulations and background was similar in the simulated and experimental time-domain data. The resulting simulated data set in the time domain is treated as the experimental one. First the decay of the background is removed, and second the data are transformed to the frequency domain with an FFT.

It is known that for azurin g-strain broadens the EPR lines at X-band frequencies and even dominates the line width at W-band frequencies.[26,27] Consequently, the effect of g-strain was considered in the simulations and incorporated in the selection procedure of the orientations of $\vec{B}_0$ that contribute to the ESEEM pattern. For each orientation of $\vec{B}_0$, B_{res} was attributed to a Lorentzian line shape with a width ΔB depending on the orientation of $\vec{B}_0$ with respect to xyz and determined by g-strain according to

$$\Delta B = (\sum_i (W_i \cos \phi_i)^2)^{1/2} \qquad i = x, y, z \quad (5)$$

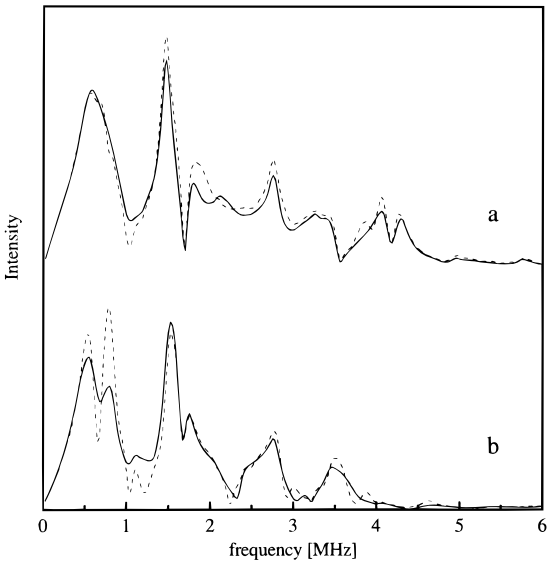

Figure 2. Simulated ESEEM spectra of azurin ($\nu = 9.748$ GHz). For the solid-line spectra g-strain was taken into account; for the dashed ones, not. Simulation a was performed for $B = 338$ mT, at the maximum of the ESE detected EPR spectrum, and simulation b for $B = 303$ mT, at the low-field edge. Spin-Hamiltonian parameters from Table 2 were used.

where the parameters W_i represent the widths of the EPR lines determined by g-strain as obtained from W-band experiments and scaled to X-band ($W_x = 0.5$, $W_y = 0.9$, $W_z = 3.8$ mT) and $\cos \phi_i$ the direction cosines between the i axes and $\vec{B}_0$. For all orientations of $\vec{B}_0$ the intensity of the Lorentzian is integrated over the interval that is spanned by the bandwidth of the microwaves and centered at B_{exp}. When for an orientation of $\vec{B}_0$ this integrated intensity is larger than 0.5% of the total integrated intensity under the Lorentzian, this orientation is selected to contribute to the modulation pattern and the subsequently calculated amplitudes at the ESEEM frequencies are weighed with the intensity integrated over the interval. In Figure 2 two examples of simulations with and without g-strain are given at different magnetic fields. Only at the extreme low-field edge of the EPR line g-strain has a significant effect on the shape of the ESEEM spectrum.

IV. Results

A. ESEEM Spectra. In Figure 3a the ESE detected EPR spectrum of azurin wild type is shown. Three-pulse ESEEM spectra of azurin are shown in Figure 3b. The magnetic field settings for these spectra are indicated by the arrows in the EPR spectrum. At high magnetic field the ESEEM spectrum is dominated by an intense and broad band at 0.80 MHz, while less intense and narrower bands are present at 1.79 and 2.82 MHz and a broad band at 4.4 MHz. At intermediate magnetic field, corresponding to the maximum of the EPR spectrum, a strong and narrow band appears at 1.51 MHz. The broad band at low frequency is less intense than at high field, and the feature around 2.8 MHz becomes more prominent. At the lowest magnetic field, bands occur at 0.70, 1.50, 2.79, and 4.3 MHz, and the band visible at about 1.8 MHz for higher fields is almost gone.

Whereas the ESEEM spectra of H117G([^{14}N]imidazole) and azurin are largely similar (cf. Figure 1), substitution of [^{15}N]-imidazole for [^{14}N]imidazole drastically changes the spectra. For H117G([^{15}N]imidazole) modulations are less deep, which leads to lower intensities of the spectra in Figure 3c. At high magnetic field the spectrum is dominated by an intense and

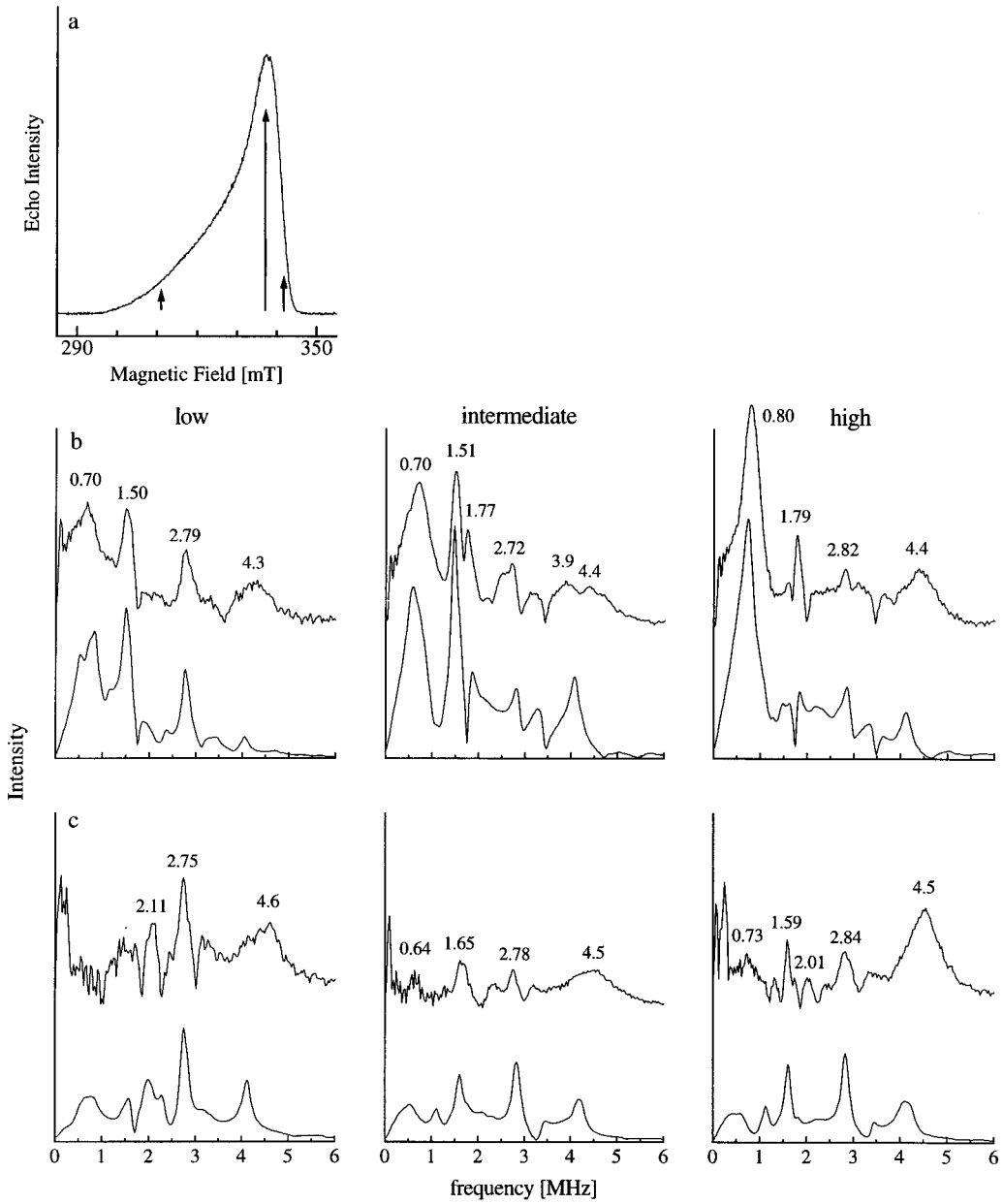

Figure 3. Experimental and simulated ESEEM spectra of frozen solutions of (b) azurin wild type and (c) H117G([^{15}N]imidazole). Low, intermediate, and high field correspond to the positions indicated by arrows in the ESE detected EPR spectrum of azurin in a. The lower curve in each panel represents the simulated spectrum. All ESEEM spectra are drawn on the same scale. They correspond to the following g-values (from left to right): (b) 2.23, 2.06, and 2.04; (c) 2.22, 2.06, and 2.04. The microwave frequencies were 9.748 GHz for b and 9.670 GHz for c. For details of the pulse sequence, see section II. Hyperfine and quadrupole tensors used in the simulations for the azurin spectra are given in Table 2. For H117G([^{15}N]-imidazole) some parameters have been slightly adjusted (cf. text). Other parameters used in the simulations: $W_x = 0.5$ mT, $W_y = 0.9$ mT, $W_z = 3.8$ mT, $A_{zz}^{Cu} = 175$ MHz, $\tau = 144$ ns, bandwidth of the microwaves = 0.3 mT, and $g_x = 2.0393$, $g_y = 2.0568$, $g_z = 2.273$.[27]

broad band at 4.5 MHz. Narrower and less intense bands appear at 1.59 and 2.84 MHz. At intermediate field the same features are present, albeit less intense and slightly shifted in frequency. At the lowest magnetic field, the band at 2.75 MHz becomes dominant and a clear feature arises at 2.11 MHz.

In Figure 4 ESEEM spectra are shown for azurin measured at the intermediate magnetic field for τ values of 144, 176, and 208 ns. Going from low to high τ values, the narrow bands at 1.51, 1.77, and 2.72 MHz gradually disappear, while the bands at 0.70 and 3.9 MHz gain intensity.

Two-dimensional ESEEM spectra are shown in Figure 5a for azurin and in Figure 5b for H117G([^{15}N]imidazole). Frequencies ν_1 and ν_2 correspond to τ and T, respectively. For azurin three strong cross-peaks are visible, indicated by I−III. Less intense cross-peaks occur at coordinates indicated by IV−VI. For H117G([^{15}N]imidazole) the cross-peaks I−III and VI are not present, which makes it possible to observe the weak correlation features indicated by VII and VIII. Cross-peak IV is still observable, while at the position of V a strong spectrometer artifact shows up which hampers the observation of a possible cross-correlation feature. The coordinates of the cross-peaks and the corresponding fundamental frequencies are summarized in Table 1.

B. Interpretation and Simulations. The two most intense bands in the ESEEM spectra of azurin are at about 0.8 and 1.5 MHz. These bands are also present in the spectra of H117G-([^{14}N]imidazole) but vanish for H117G([^{15}N]imidazole), where the ^{14}N nuclei ($I = 1$) are replaced by ^{15}N ($I = {}^1/_2$) at the

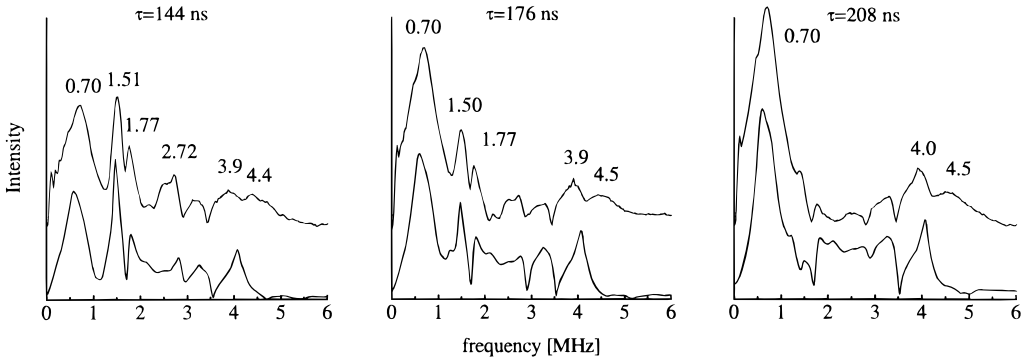

Figure 4. Experimental and simulated ESEEM spectra for azurin wild type at the intermediate magnetic field for different τ values. The upper traces are the experimental spectra. The microwave frequency was 9.748 GHz. The parameters used in the simulations are given in the caption of Figure 3 and in Table 2.

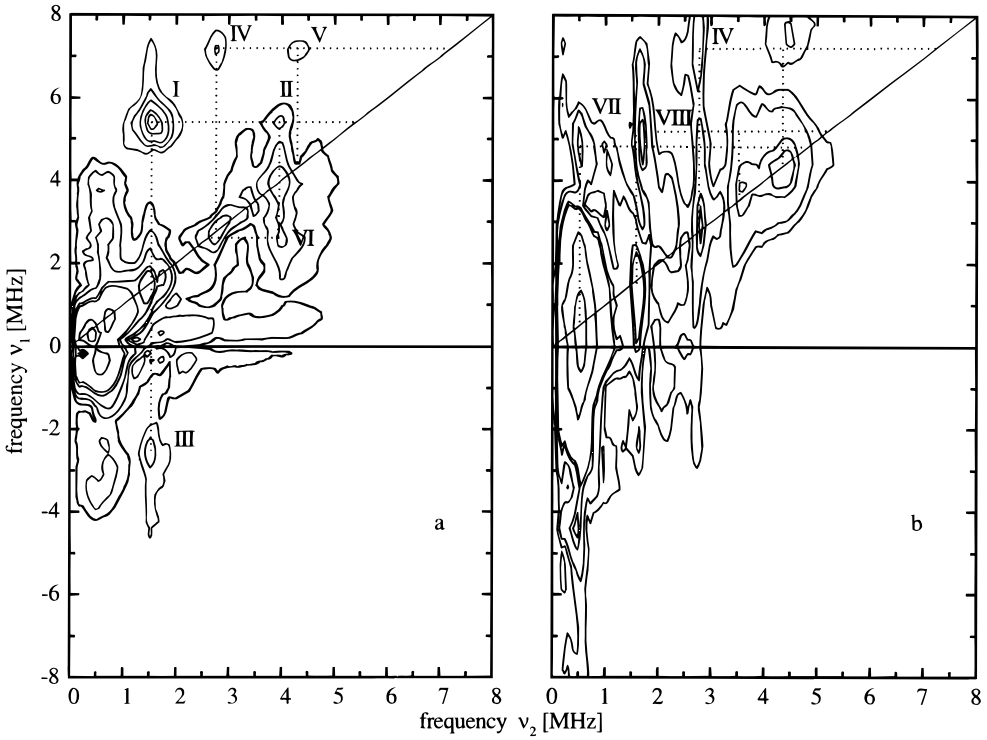

Figure 5. Two-dimensional ESEEM spectra of (a) azurin wild type and (b) H117G([^{15}N]imidazole) measured at intermediate magnetic field. The microwave frequencies are the same as in the experiments shown in Figure 3. The Roman numerals label the cross-peaks (cf. Table 1).

TABLE 1: Cross-Correlation Peaks (ν_1, ν_2) in the 2D ESEEM Spectra of Azurin and H117G([^{15}N]Imidazole) (cf. Figure 5) and the Corresponding Fundamental Frequencies[a]

cross-peak		fundamental freq		cross-peak		fundamental freq	
I	(5.5, 1.5)	1.5	4.0	IV	(7.1, 2.8)	2.8	4.3
II	(5.5, 4.0)	1.5	4.0	V	(7.1, 4.3)	2.8	4.3
III	(−2.5, 1.5)	1.5	4.0	VII	(4.8, 0.5)	0.5	4.3
VI	(2.5, 4.0)	1.5	4.0	VIII	(5.2, 1.7)	1.7	3.5

[a] The first coordinate represents the τ related combination frequency and the second coordinate the T related fundamental frequency. Cross-peaks I−III are most intense, IV and V are less intense, and VI−VIII are weak features.

histidine-117 position. Consequently, these bands are attributed to the remote nitrogen of histidine-117. The 0.8 and 1.5 MHz frequencies are similar to the quadrupole frequencies for the protonated nitrogen of solid imidazole.[28] From these frequencies the quadrupole parameters η and e^2qQ/h can be estimated to be 1.0 and −1.5 MHz (note that the sign of e^2qQ is inferred from calculations of the electric field gradient[29]). In Figure 5a cross-peaks I−III and VI correlate the frequencies 1.5 and 4.0 MHz (cf. Table 1). In 2D ESEEM cross-peaks relate a combination frequency to a fundamental frequency and are expected at ($\nu_Q \pm \nu_{DQ}$, ν_Q) and ($\nu_{DQ} \pm \nu_Q$, ν_{DQ})[30] where ν_Q represents one out of the three frequencies in the canceled manifold and ν_{DQ} the $\Delta M_I = 2$ frequency. Cross-peaks I, III, II, and VI are observed at respectively (1.5 + 4.0, 1.5), (1.5 − 4.0, 1.5), (4.0 + 1.5, 4.0), and (4.0 − 1.5, 4.0) corresponding to $\nu_Q = 1.5$ MHz and $\nu_{DQ} = 4.0$ MHz. Consequently, the cross-peaks indicate that the $\Delta M_I = 2$ transition of the remote nitrogen of histidine-117 occurs at 4.0 MHz at the intermediate field strength.

Except for the histidine-117 related part, the ESEEM spectrum of azurin should be nearly identical to that of H117G([^{15}N]-imidazole) as the ^{15}N nucleus at the histidine-117 position only contributes to the low-frequency part of the ESEEM spectra of H117G([^{15}N]imidazole) (vide infra). The number of bands present in the spectra of H117G([^{15}N]imidazole), Figure 3c, is incompatible with contributions of the remote nitrogen of histidine-46 alone. Consequently, the ESEEM spectra of

TABLE 2: Principal Values (MHz) of the Hyperfine and Quadrupole Tensors and Orientations of the Principal Axes of the Hyperfine ($x''y''z''$) and Quadrupole ($x'y'z'$) Tensors with Respect to the Principal Axes System of the g-Tensor (xyz) As Used in the Simulations of the ESEEM Spectra of Azurin[a]

	a_{iso}/h	$A_{x''x''}$/h	$A_{y''y''}$/h	$A_{z''z''}$/h		x	y	z
Nϵ His117	1.40 [1.30]	1.76 [1.65]	1.36 [1.26]	1.07 [0.98]	x''	−0.333 [−0.440]	−0.939 [−0.897]	0.091 [0.040]
					y''	0.644 [0.557]	−0.156 [−0.316]	−0.749 [−0.753]
					z''	0.689 [0.689]	−0.308 [−0.308]	0.657 [0.657]
Nϵ His46	0.97 [0.87]	1.11 [1.10]	1.00 [0.80]	0.79 [0.69]	x''	[0.843]	[−0.522]	[0.131]
					y''	[−0.520]	[−0.726]	[0.449]
					z''	[−0.140]	[−0.447]	[−0.884]
N backbone (Cys 112)	−0.95 [0.95]	−1.14 [1.14]	−1.02 [1.02]	−0.68 [0.68]	x''	0.583 [0.754]	0.428 [0.657]	−0.691 [0.020]
					y''	−0.653 [−0.653]	0.752 [0.752]	−0.085 [−0.085]
					z''	0.483 [−0.071]	0.501 [0.051]	0.718 [0.996]

	e^2qQ/h	η	$Q_{x'x'}$	$Q_{y'y'}$	$Q_{z'z'}$				
Nϵ His117	−1.38 [−1.43]	1.10 [0.95]	−0.03 [0.02]	0.72 [0.70]	−0.69 [−0.72]	x'	−0.240 [−0.145]	−0.762 [−0.867]	−0.601 [−0.476]
						y'	0.797 [0.887]	0.199 [0.099]	−0.571 [−0.452]
						z'	0.555 [0.439]	−0.616 [−0.488]	0.559 [0.755]
Nϵ His46	−1.47 [−1.37]	0.86 [0.86]	0.05 [0.05]	0.68 [0.64]	−0.74 [−0.68]	x'	[0.482]	[−0.798]	[0.362]
						y'	[0.014]	[−0.407]	[−0.914]
						z'	[0.876]	[0.446]	[−0.185]
N backbone (Cys 112)	−3.10	0.40	0.47	1.09	−1.55	x'	−0.601	−0.626	0.497
						y'	0.353	0.351	0.867
						z'	−0.717	0.697	0.010

[a] The values between square brackets stem from the pulsed ENDOR study on single crystals of azurin.[32] The definition of the principal axes $x'y'z'$ for Nϵ His117 deviates from the convention $|Q_{z'z'}| > |Q_{y'y'}| > |Q_{x'x'}|$. This facilitates the comparison of the quadrupole tensor with previous ENDOR data but leads to a value of η larger than 1. From the simulations of the ESEEM spectra of H117G([^{15}N]imidazole) slightly different values were found compared to those for azurin: for the histidine-46 remote nitrogen −1.31 MHz for e^2qQ and 0.87 MHz for a_{iso}, for the backbone nitrogen −1.05 MHz for a_{iso}. Comparison of experimental ESEEM spectra with simulations while systematically varying one parameter resulted in the following error margins: ±0.1 MHz for the principal values of the hyperfine and quadrupole tensors, ±10° for the orientations of the principal axes of these tensors for both remote nitrogens, and ±15° and ±25° for the orientations of the principal axes of the quadrupole and hyperfine tensors of the backbone nitrogen.

H117G([^{15}N]imidazole) and of azurin derive not only from interactions of the electron spin with the remote nitrogens of the coordinated histidines. In the spectra of H117G([^{15}N]-imidazole) bands are visible at frequencies of about 0.7, 2.1, and 2.8 MHz. The band at 2.8 MHz is even most intense at the lowest magnetic field. The bands are relatively sharp, and the two lower frequencies add up to the highest one, which suggests that these frequencies belong to the same nitrogen nucleus. The quadrupole parameters corresponding to these frequencies are 0.4 and 3.3 MHz for η and e^2qQ/h, respectively. Such quadrupole parameters are unlike those obtained for remote nitrogens in imidazoles[11,27] but alike those observed for nitrogens in a backbone(-like) configuration.[31,32] Therefore we ascribe these frequencies to a backbone nitrogen. Furthermore, cross-peaks IV and V in Figure 5 correlate 2.8 MHz to 4.3 MHz while correlation peak VII correlates 0.5 MHz to 4.3 MHz. Thus, the $\Delta M_I = 2$ transition of the backbone nitrogen is expected around 4.3 MHz.

The backbone nitrogen accounts for most of the frequencies in the ESEEM spectra of H117G([^{15}N]imidazole). One feature that is not accounted for is the band at about 1.7 MHz, clearly present at high magnetic field, whose intensity slightly decreases when going to lower magnetic field. Most probably this band stems from the remote nitrogen of histidine-46. Cross-peak VIII in Figure 5b correlates 1.7 and 3.5 MHz, which indicates that the corresponding $\Delta M_I = 2$ transition has a frequency of 3.5 MHz.

The ESEEM spectra of frozen solutions of azurin and of H117G([^{15}N]imidazole) seem to show contributions from the remote nitrogens of histidine-117 (only for azurin) and histidine-46 and from a backbone nitrogen. To substantiate this interpretation, simulations have been performed. A pulsed ENDOR study of single crystals of [^{14}N]- and [^{15}N]azurin[33] provided for a set of hyperfine and quadrupole parameters that have been used as starting values. This concerned the hyperfine tensors and the orientations of the principal axes of the quadrupole tensors (with respect to the **g**-tensor principal axes xyz) for the remote nitrogens of the histidines and the hyperfine tensor for the backbone nitrogen (cf. Table 1 of ref 32). Subsequently, parameters have been varied to optimize the descriptions of the ESEEM spectrum of the frozen solution of azurin in terms of contributions of the three nuclei mentioned above and of the ESEEM spectrum of the frozen solution of H117G([^{15}N]imidazole) in terms of contributions of the backbone nitrogen and the remote nitrogen of histidine-46. The resulting simulations, represented in Figure 3, confirm that an adequate description of the ESEEM spectra of azurin and H117G([^{15}N]imidazole) has been obtained. The corresponding hyperfine and quadrupole tensors are summarized in Table 2. Simulations of the ESEEM spectra of azurin at intermediate magnetic field for different τ values using these parameters are shown in Figure 4. Note that the sign of the hyperfine interaction of the backbone nitrogen is found to be opposite to that of the remote nitrogens. The different sign has almost no effect on the simulations of the H117G([^{15}N]imidazole) spectra but resulted in a better relative intensity of the 2.8 MHz band of the backbone nitrogen compared to that of the quadrupole lines of the remote nitrogen of histidine-117 in the simulations of azurin. The relative intensities depend on the relative sign of the hyperfine interaction of the nuclei, which is related to the fact that the amplitudes corresponding to the frequencies in the two electron-spin manifolds are multiplied separately in the product formula (cf. eq 4).

V. Discussion

Comparison of the ESEEM spectra of azurin and H117G-([^{15}N]imidazole) with spectral simulations reveals that, besides the expected occurrence of signals of the remote nitrogens of histidines-46 and -117, a backbone nitrogen contributes sub-

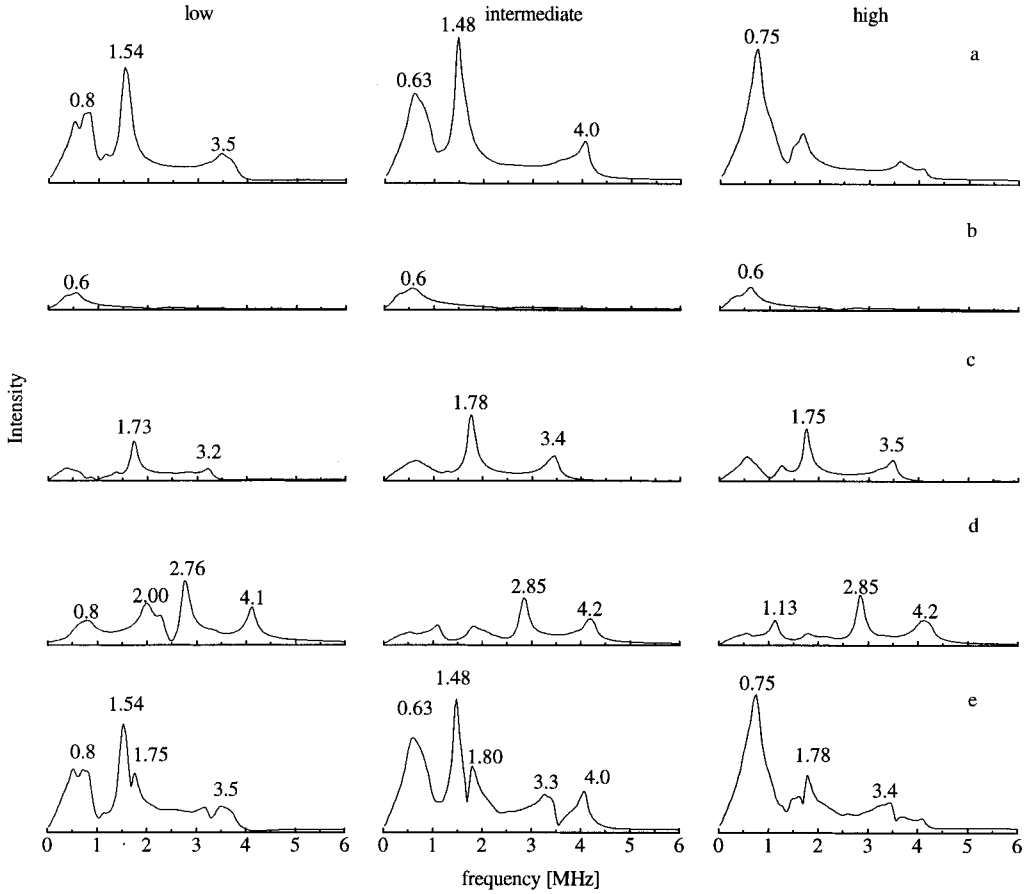

Figure 6. Single-nucleus simulations for (a) the remote nitrogen of histidine-117, (b) the ^{15}N nucleus, (c) the remote nitrogen of histidine-46, and (d) the backbone nitrogen, and two-nuclei simulations including both remote nitrogens (e). The hyperfine and quadrupole tensors used for a and c−e are represented in Table 2. The hyperfine tensor of the remote nitrogen of histidine-117 from Table 2 was used in b, after correction for the nuclear g-value of ^{15}N. Other simulation parameters are given in the caption of Figure 3. For a−c and e $\nu = 9.748$ GHz, and for d $\nu = 9.670$ GHz. All simulations are drawn on the same scale.

stantially to the modulation pattern of azurin. This recognition has enabled a full assignment of the ESEEM spectra, and simulations allowed us to assign the ESEEM frequencies to the respective nuclei. Here we discuss the contributions of these nuclei to the spectra of azurin and H117G([^{15}N]imidazole) one by one.

The most conspicuous contribution to the modulation pattern of azurin is that of the remote nitrogen of histidine-117. Comparison of the experimental ESEEM spectra of azurin and H117G([^{15}N]imidazole) shows that the quadrupole frequencies at 0.8 and 1.5 MHz arise from this nitrogen and the corresponding bands dominate the azurin spectrum. Intense quadrupole bands with comparable frequencies have been observed for remote nitrogens in copper imidazole complexes and in the blue-copper sites of laccase and ascorbate oxidase.[8,11,34] Simulations of the contributions of individual nuclei to the ESEEM spectra, based on the same parameters as used for the simulations in Figure 3 (cf. Table 2) are shown in Figure 6. These simulations confirm that the modulation depth is largest for the remote nitrogen of histidine-117 (Figure 6a). The hyperfine interaction of this nucleus is significantly larger and closer to the cancellation condition than that of the other two nuclei yielding deeper modulations. The low-frequency band contains two transitions that nearly coincide ($\eta \approx 1$). The shape of the $\Delta M_I = 2$ band for this nucleus varies with field. The band is narrowest in the simulation at the intermediate field strength with an intensity maximum at 4.0 MHz, corresponding to the position derived from the cross-peaks in the 2D ESEEM spectrum. The simulations for ^{15}N at the position of the remote nitrogen of histidine-117 are shown in Figure 6b. For these simulations the hyperfine tensor of the remote nitrogen of histidine-117 (cf. Table 2) was used after correction for the different nuclear g-values of ^{14}N and ^{15}N. Of the two frequencies possible for ^{15}N ($I = {}^1/_2$), only the one below 1 MHz shows significant intensity. Consequently, for H117G([^{15}N]imidazole) the ^{15}N nucleus contributes only slightly to the ESEEM spectrum in the low-frequency region.

The contribution of the second remote nitrogen, that of histidine-46, to the ESEEM spectra of azurin is markedly different from that of the remote nitrogen of histidine-117. The simulations for this nitrogen in Figure 6c show that only one of the quadrupole bands, the one at about 1.8 MHz, has considerable intensity. At the X-band frequencies used in this study, the remote nitrogen of histidine-46 is further away from cancellation than the remote nitrogen of histidine-117 and its contribution to the ESEEM spectra is limited. Consequently, we have not been able to optimize the orientations of the hyperfine and quadrupole principal axes for this nucleus. As far as these parameters are concerned, the simulations in Figures 3, 4, and 6c,e are based on the values obtained from the ENDOR study on single crystals of azurin. Slightly different optimized values of e^2qQ and a_{iso} for the remote nitrogen of histidine-46 have been found for the wild type and the reconstituted site: −1.47 and 0.97 MHz for azurin compared to −1.31 and 0.87 MHz for H117G([^{15}N]imidazole). This inequivalence is evident from a comparison of the ESEEM spectra in Figure 3b,c, where

the histidine-46 related band around 1.8 MHz shows up about 0.2 MHz lower in frequency for H117G([^{15}N]imidazole) than for azurin and from Figure 1 where the shoulder around 1.8 MHz is more pronounced for azurin than for H117G([^{14}N]-imidazole). These changes in e^2qQ and a_{iso}, although small, point to a subtle change in the electron distribution around this nitrogen.

One of the, at first sight, difficult to interpret bands in the ESEEM spectrum of azurin concerned the one at 2.8 MHz. We have assigned this band to a backbone nitrogen based on the principal values of the quadrupole tensor. Single-nucleus simulations for this nitrogen, shown in Figure 6d, nicely reproduce the 2.8 MHz band and the position of the $\Delta M_I = 2$ transition at 4.2 MHz, in agreement with the 2D ESEEM result. In addition, this simulation shows that the contribution of this nucleus is comparable to that of the remote nitrogen of histidine-46 and even larger at the low-field edge (cf. Figures 6c,d). In view of its frequency, one might in first instance have considered the 2.8 MHz band to be a combination band related to the quadrupole lines of the remote nitrogens of the two histidines. Such an interpretation, besides being incompatible with the occurrence of this band in the spectra of H117G([^{15}N]imidazole) fails, because the modulation depth for the remote nitrogen of histidine-46 is too low to yield appreciable intensity for combination bands. Comparison of the simulated spectra in Figure 6e, including the two histidine nitrogens, with those in Figure 6a,c confirms the marginal contribution of such combination bands to the ESEEM spectra of azurin. This in contrast to ESEEM studies for systems where the contributing nitrogens all are about equally well canceled and strong combination bands have been observed.[13]

Although the simulations nicely reproduce nearly all features in the azurin and H117G([^{15}N]imidazole) ESEEM spectra (cf. Figure 3), the agreement between experiment and simulation is not perfect. Some imperfections are to be expected because of simplifications in the density-matrix formalism. First, the microwave pulses are taken to be ideal δ pulses. The theory of ESEEM including nonideality of the microwave pulses has been described recently.[35] The assumption of ideal pulses influences the shape and intensity of the bands at fundamental frequencies. Second, no relaxation effects are included in the formalism. We implemented the decay of the background and the modulations by multiplying the time-domain data by two exponentials. Consequently, the decay of all frequencies in the ESEEM pattern was taken as being identical, which is actually not the case. This affects the relative intensities and the line widths in the spectrum. In addition, the removal of the background introduces uncertainty with regard to the low-frequency part of the spectrum (up to 0.5 MHz). It is conceivable that hyperfine and quadrupole strains[33] ought to be included in the simulations because these strain mechanisms might well-affect the ESEEM line widths more than *g*-strain. A particular mismatch between experimental and simulated spectra in Figures 3 and 4 concerns the band around 4.5 MHz. The experimental spectra consistently show a band that is broader and more intense and contain a maximum at higher frequency than the corresponding simulations. In those cases where the experimental band shape is double-humped, the simulations reproduce the low-frequency part which is particularly visible in the spectra for different τ values in Figure 4. In addition, the simulated position of the $\Delta M_I = 2$ transition corresponds for all three nitrogens to the frequency derived from the 2D ESEEM spectra (cf. Table 1). These observations suggest that the high-frequency part of the 4.5 MHz band in the experimental spectra does not belong to the $\Delta M_I = 2$ transition of any of the nitrogen nuclei taken into account. Its origin remains unclear so far.

In the simulations of ESEEM spectra of copper complexes in the literature much attention is often paid to the $\Delta M_I = 2$ bands and conclusions are drawn with regard to the isotropic and anisotropic hyperfine interaction from the frequency and the line shape of these bands.[36−38] The present observations suggest some caution in this respect. If more nitrogen nuclei are present, the $\Delta M_I = 2$ band is composed of several contributions with distinct frequencies. Moreover, when the anisotropic hyperfine interaction of a histidine remote nitrogen is determined from the line shape of the $\Delta M_I = 2$ transition, it is usually approximated to be axial.[36,37] As is clear from Table 2, this certainly is not true for azurin, where one principal value of the anisotropic hyperfine tensors is invariably close to zero. The nonaxiality of the hyperfine tensor can lead to complicated line shapes for the $\Delta M_I = 2$ feature, as is nicely illustrated by the single-nucleus simulation in Figure 6a at high magnetic field where the $\Delta M_I = 2$ feature reveals even two intensity maxima.

Finally, the hyperfine and quadrupole data obtained from ESEEM for azurin in frozen solution are compared with those from pulsed ENDOR for a single crystal of azurin. In Table 2 the latter data are represented in square brackets. For the two remote nitrogens small differences show up in the principal values and, as far as histidine-117 is concerned, in the orientation of the principal axes which are on the order of the error margin in both experiments. Consequently, the coordination of the histidines in the copper site in solution and crystal is virtually identical. The data for the backbone nitrogen deserve a more extensive discussion. Following the first recognition of a contribution of a backbone nitrogen to the ESEEM spectrum of azurin, it was suggested that this nitrogen might concern the backbone nitrogen of either cysteine-112 or histidine-46.[18] Subsequently, the pulsed ENDOR data of the single crystal in combination with the theoretical prediction that the quadrupole z′ axis should be perpendicular to the C−N−C backbone fragment led us to the assignment of the backbone nitrogen as that of cysteine-112[33]. Meanwhile Kofman et al.[39] suggested an assignment in terms of histidine-46 based on a comparison of azurin with ascorbate oxidase. The present ESEEM results show (i) a hyperfine tensor of the backbone nitrogen whose principal x'' and z'' axes are rotated about 45° with respect to their orientation in the crystal, (ii) a quadrupole tensor of the backbone nitrogen for which the orientation of the principal axes is different from that for the crystal (incompletely known in the latter case), and (iii) an orientation of the quadrupole z' axis that is not perpendicular to the plane of the C−N−C backbone fragment of cysteine-112 (nor to that of histidine-46), but makes an angle of about 30° degrees with the normal to that plane, assuming the orientation of the backbone plane to be identical for azurin in the crystal and in the frozen solution. These considerations lead us to suggest that the orientation of the cysteine-112 backbone fragment in solution is different from that in the crystal, while the histidine-46 and histidine-117 parts of the copper site seem to be highly conserved. This reorientation as well as the extent of the electron-spin delocalization over the cysteine ligand are presently under investigation in our laboratory.

In conclusion we emphasize that a quantitative analysis of the X-band ESEEM spectra of a frozen solution of azurin has been achieved. Simulations show that the remote nitrogen of histidine-117 dominates the ESEEM spectrum of azurin and that the contribution of the remote nitrogen of histidine-46 is

relatively minor, because the hyperfine interaction for the remote nitrogen of histidine-117 is about 1.5 times bigger than for the remote nitrogen of histidine-46. With the aid of the ESEEM spectra of H117G([^{15}N]imidazole), their simulation, and the 2D ESEEM spectra the contribution of a backbone nitrogen to the ESEEM spectrum of azurin has been recognized. The presence of signals from this backbone nitrogen, most probably that of cysteine-112, in the ESEEM spectra of azurin nicely brings out the delocalized character of the unpaired electron wave function. In addition it shows that in the analysis of the ESEEM spectra of blue-copper proteins not only the remote nitrogens of the histidines should be considered. Care should be taken in drawing conclusions with regard to copper coordination from ESEEM spectra.

Acknowledgment. This work has been performed under the auspices of the Biomac Research School of the Leiden and Delft Universities and was supported by The Netherlands Foundation for Chemical Research (SON) with financial aid from The Netherlands Organization for Scientific Research (NWO) and the ABON foundation.

References and Notes

(1) Sykes, A. G. *Adv. Inorg. Chem.* **1991**, *36*, 377−408.
(2) Mims, W. B.; Peisach, J. *Biochemistry* **1976**, *15*, 3863−3869.
(3) Mondovi, B.; Graziani, M. T.; Mims, W. B.; Oltzik, R.; Peisach, J. *Biochemistry* **1977**, *16*, 4198−4201.
(4) Mims, W. B.; Peisach, J.; Shaw, R. W.; Beinert, H. *J. Biol. Chem.* **1980**, *255*, 6843−6846.
(5) Kosman, D. J.; Peisach, J.; Mims, W. B. *Biochemistry* **1980**, *19*, 1304−1308.
(6) Colaneri, M. J.; Peisach, J. *J. Am. Chem. Soc.* **1995**, *117*, 6308−6315.
(7) Peisach, J. In *Bioinorganic chemistry of copper*; Karlin, K. D., Tyeklar, Z., Eds.; Chapman & Hall: New York, 1993; pp 21−33.
(8) Goldfarb, D.; Fauth, J. M.; Farver, O.; Pecht, I. *Appl. Magn. Reson.* **1992**, *3*, 333−351.
(9) Dikanov, S. A.; Spoyalov, A. P.; Hüttermann, J. *J. Chem. Phys.* **1994**, *100*, 7973−7983.
(10) Gerfen, G. J.; Singel, D. J. *J. Chem. Phys.* **1994**, *100*, 4127−4137.
(11) Jiang, F.; McCracken, J.; Peisach, J. *J. Am. Chem. Soc.* **1990**, *112*, 9035−9044.
(12) Flanagan, H. L.; Singel, D. J. *J. Chem. Phys.* **1987**, *87*, 5606−5616.
(13) McCracken, J.; Pember, S.; Benkovic, S. J.; Villafranca, J. J.; Miller, R. J.; Peisach, J. *J. Am. Chem. Soc.* **1988**, *110*, 1069−1074.
(14) Baker, E. N. *J. Mol. Biol.* **1988**, *203*, 1071−1095.
(15) Nar, H.; Messerschmidt, A.; Huber, R.; van de Kamp, M.; Canters, G. W. *J. Mol. Biol.* **1991**, *221*, 765−772.
(16) Mims, W. B.; Davis, J. L.; Peisach, J. *Biophys. J.* **1984**, *45*, 755−766.
(17) Lu, J.; Bender, C. J.; McCracken, J.; Peisach, J.; Severns, J. C.; McMillin, D. R. *Biochemistry* **1992**, *31*, 6265−6272.
(18) Coremans, J. W. A.; van Gastel, M.; Poluektov, O. G.; Groenen, E. J. J.; den Blaauwen, T.; van Pouderoyen, G.; Canters, G. W.; Nar, H.; Hamman, C.; Messerschmidt, A. *Chem. Phys. Lett.* **1995**, *235*, 202−210.
(19) den Blaauwen, T.; van de Kamp, M.; Canters, G. W. *J. Am. Chem. Soc.* **1991**, *113*, 550−552.
(20) den Blaauwen, T.; Canters, G. W. *J. Am. Chem. Soc.* **1993**, *115*, 1121−1129. The *g* and *A* values for H117G(imidazole) and H117G(thiazole) in Table 1 of this reference are in error. The correct values are similar to those for azurin.
(21) van de Kamp, M.; Hali, F. C.; Rosato, N.; Finazzi Agro, A.; Canters, G. W. *Biochim. Biophys. Acta* **1990**, *1019*, 283−292.
(22) Gemperle, C.; Aebli, G.; Schweiger, A.; Ernst, R. R. *J. Magn. Reson.* **1990**, *88*, 241−256.
(23) de Beer, R.; van Ormondt, D. In *Advanced EPR: Applications in Biology and Biochemistry*; Hoff, A. J., Ed.; Elsevier: Amsterdam, 1989; pp 135−176.
(24) Mims, W. B. *Phys. Rev. B* **1972**, *5*, 2409−2419.
(25) Mims, W. B. *Phys. Rev. B* **1972**, *6*, 3543−3545.
(26) Groeneveld, C. M.; Aasa, R.; Reinhammar, B.; Canters, G. W. *J. Inorg. Biochem.* **1987**, *31*, 143−154.
(27) Coremans, J. W. A.; Poluektov, O. G.; Groenen, E. J. J.; Canters, G. W.; Nar, H.; Messerschmidt, A. *J. Am. Chem. Soc.* **1994**, *116*, 3097−3101.
(28) Hunt, M. J.; MacKay, A. L.; Edmonds, D. T. *Chem. Phys. Lett.* **1975**, *34*, 473−475.
(29) Palmer, M. H.; Scott, F. E.; Smith, J. A. S. *Chem. Phys.* **1983**, *74*, 9−14.
(30) Shane, J. J.; Höfer, P.; Reijerse, E. J.; de Boer, E. *J. Magn. Reson.* **1992**, *99*, 596−604.
(31) Rabbani, S. R.; Edmonds, D. T.; Gosling, P. *J. Magn. Reson.* **1987**, *72*, 230−237.
(32) Palmer, M. H. *Z. Naturforsch.* **1984**, *39a*, 1108−1111.
(33) Coremans, J. W. A.; Poluektov, O. G.; Groenen, E. J. J.; Canters, G. W.; Nar, H.; Messerschmidt, A. *J. Am. Chem. Soc.* **1996**, *118*, 12141−12153.
(34) Avigliano, L.; Davis, J. L.; Graziani, M. T.; Marchesini, A.; Mims, W. B.; Mondovi, B.; Peisach, J. *FEBS Lett.* **1981**, *136*, 80−84.
(35) Jeschke, G.; Schweiger, A. *Mol. Phys.* **1996**, *88*, 355−383; *J. Chem. Phys.* **1996**, *105*, 2199−2211.
(36) Jiang, F.; Karlin, K. D.; Peisach, J. *Inorg. Chem.* **1993**, *32*, 2576−2582.
(37) Jiang, F.; Peisach, J.; Ming, L. J.; Que, L.; Chen, V. J. *Biochemistry* **1991**, *30*, 11437−11445.
(38) Warncke, K.; Brooks, H. B.; Lee, H.; McCracken, J.; Davidson, V. L.; Babcock, G. T. *J. Am. Chem. Soc.* **1995**, *117*, 10063−10075.
(39) Kofman, J.; Farver, O.; Goldfarb, D. *J. Am. Chem. Soc.* **1996**, *118*, 1201−1206.